Crystal structures of taxane-tubulin complexes: Implications for the mechanism of microtubule stabilization by Taxol

Andrea E. Prota[1*]; Daniel Lucena-Agell[2¤]; Yuntao Ma[3¤]; Juan Estévez-Gallego[2¤]; Carlos Roca[4]; Fernando Josa-Prado[2]; Kenneth Goossens[2‡]; Juan Francisco Giménez-Abián[2], Shuo Li[3], Ángeles Canales[2,4]; Katja Bargsten[1+]; José Manuel Andreu[2]; Karl-Heinz Altmann[5]; Natacha Olieric[1]; Shinji Kamimura[6]; Tobias Mühlethaler[1]; María A. Oliva.[2]; Michel O. Steinmetz[1,7]; Wei-Shuo Fang[3*]; J. Fernando Díaz[2*].

[1]Laboratory of Biomolecular Research, Division of Biology and Chemistry, Paul Scherrer Institut, CH-5232 Villigen, Switzerland

[2]Centro de Investigaciones Biológicas Margarita Salas, Consejo Superior de Investigaciones Científicas, Ramiro de Maeztu 9, 28040 Madrid, Spain

[3]State Key Laboratory of Bioactive Substances and Functions of Natural Medicines, Institute of Materia Medica, Chinese Academy of Medical Sciences & Peking Union Medical College, 2A Nan Wei Road, Beijing 100050, China

[4]Department of Organic Chemistry, Faculty of Chemistry, Universidad Complutense de Madrid. Av. Complutense, s/n, 28040 Madrid

[5]Department of Chemistry and Applied Biosciences, Institute of Pharmaceutical Sciences, ETH, Zürich, Vladimir-Prelog Weg 4, HCI H405, CH-8093 Zürich, Switzerland

[6]Department of Biological Sciences, Faculty of Science and Engineering, Chuo University, Kasuga, Bunkyo, Tokyo, Japan

[7]University of Basel, Biozentrum, 4056 Basel, Switzerland

[‡]Current address: Department of Pharmaceutical Sciences, Laboratory of Medicinal Chemistry, University of Antwerp, Universiteitsplein 1, 2610 Wilrijk, Belgium.

[+]Current address: leadXpro AG, PARK innovAARE, CH-5234 Villigen, Switzerland

[¤]These authors have equally contributed to this work.

[*]Corresponding Authors. andrea.prota@psi.ch; wfang@imm.ac.cn; fer@cib.csic.es

Abstract

Paclitaxel (Taxol®) is a first-line chemotherapeutic drug that promotes the curved-to-straight conformational transition of tubulin, an activation step that is necessary for microtubule formation. Crystallization of Taxol bound to tubulin has been long elusive. We found that baccatin III, the core structure of paclitaxel which lacks the C13 side chain, readily co-crystallizes with curved tubulin. Tailor-made taxanes with alternative side chains also co-crystallized, allowing us to investigate their binding modes. Interestingly, these Taxol derived compounds lost their microtubule stabilizing activity and cytotoxicity but kept their full microtubule binding affinity, and all induced lattice expansion upon binding. Additional nuclear magnetic resonance studies propose that Taxol binds to a small fraction of straight tubulin present in solution. Our results suggest a mode of action of Taxol, where the core structure is responsible for the interacting energy while the bulky hydrophobic C13 side chain enables binding selectively to straight tubulin and promotes stabilization.

Introduction

Taxanes are the main choice among other chemotherapeutic agents for the treatment of several solid tumors such as ovarian, lung and breast cancer, as well as advanced Kaposi's sarcoma(*1*). The three active taxanes in clinical use, paclitaxel (Taxol®; Ptx), docetaxel (Taxotere®; Dcx) and cabazitaxel (Jevtana®), are part of a big family of chemically diverse compounds that bind to the taxane site of the αβ-tubulin heterodimer(*2*) **(Fig. 1A)**. This family of compounds also includes other non-taxane molecules and a wide range of analogs derived thereof. Because taxane-site targeting compounds promote tubulin assembly into microtubules (MTs)(*3*), they are called MT-stabilizing agents (MSAs). From the thermodynamic point of view, taxane-site MSAs contribute to MT assembly by their preferred binding to them(*4*). Tubulin displays two known conformations, related to its assembly state: a straight conformation (s-tubulin) present in MTs and zinc-induced sheets(*5, 6*), and a curved conformation (c-tubulin) observed in unassembled tubulin, which is non-related to the nucleotide bound to the regulatory site of β-tubulin (GTP or GDP)(*7, 8*). The curved-to-straight conformational transition is required for MT-assembly. Current hypotheses(*9-11*) establish that the activation of tubulin for assembly could be accomplished by different pathways and each MSA could favor a specific one, depending on its structure and its interaction pattern with unassembled, c-tubulin. Structural studies of taxane-site agents(*10, 12*) bound to MTs or unassembled tubulin have shed light on the binding mode to s- and c-tubulin tubulin, respectively. Nevertheless, their underlying mechanisms of action are still a matter of debate. On one hand, zampanolide and epothilone induce the complete restructuring of the βM-loop in unassembled, c-tubulin **(Fig. 1B)**, which is a key secondary structural element required for the stabilization of lateral contacts between protofilaments (PF) within the MT(*12*). These compounds mainly connect the base of the βM-loop with both the N-terminal domain helix βH6 and the central helix βH7 (**Fig. 1B**), similarly to dictyostatins and discodermolides(*9, 13*). However, neither dictyostatins nor discodermolides fold the βM-loop into a helix, which suggests a different mechanism. The interaction of Ptx with MTs affects the longitudinal tubulin interface along protofiliaments (PFs), increasing the axial repeat of tubulin dimers (i.e., causing a lattice expansion)(*10*). The stabilizing effect promoted in assembled, s-tubulin involves subtle movements in the N-terminal domain helix βH1, the central helix βH7 and the intermediate domain loop βS9-βS10 (**Fig. 1B**)(*10*). However, the molecular details of

how Ptx favors these movements and promotes MT assembly and stabilization are unknown yet.

Ptx is one of the drugs in the World Health Organization's List of Essential Medicines, but the appearance of side effects (e.g., neurotoxicity) compromises chemotherapy cycles during cancer treatment. Understanding the underlying mechanism of MT stabilization by taxanes is highly required to lay the groundwork for future and safer drugs. To date, all efforts to obtain high-resolution crystal structures and hence, detailed information on the Ptx, Dcx or cabazitaxel interacting network within the taxane-site have been unssucessful(*7, 8, 14*). Here, we have taken a multidisciplinary approach to unveil how Ptx recognizes the taxane site and stabilizes MTs. From the Ptx core structure (baccatin III) to specifically tailored Ptx derivatives with alternative engineered C13 tails, we have combined macromolecular crystallographic high-resolution structures with biochemical, cell biology, nuclear magnetic resonance (NMR) and X-ray fiber diffraction studies to explain how clinically used taxanes induce MT assembly from c-tubulin and how they stabilize MTs.

Results

The bulky group at ring A position of the C13 side chain precludes binding to curved conformation and is essential for activity.

To determine the high-resolution structure of a taxane bound to tubulin we performed both soaking and co-crystallization experiments using the previously described crystal system consisting of a protein complex composed of two αβ-tubulin heterodimers, the stathmin-like protein RB3 and the tubulin tyrosine ligase (termed T_2R-TTL)(*12, 14*) as well as with the DARPin D1-tubulin crystal system (TD1)(*8*). Upon failure with a first series of tested taxanes comprising Ptx, Dcx, the more soluble 3'N-aminopaclitaxel (N-AB-PT, **Fig. 1C**)(*15*) and the engineered high affinity taxanes Chitax 40(*16*) and Chitax 68(*17*) (**Fig. 1C**), we approached the challenge from a different angle. We started with baccatin III, a precursor in the biosynthesis of Ptx that contains both the C2-benzoyloxy ring C and the C10 acetate ester, but lacks the C13 side chain with both the 3'-N-benzamido phenyl ring A and the 3'-phenyl ring B moieties(*18*).

Baccatin III (**Fig. 1C**) is reported to be biologically inactive(*19-21*) despite of having μM affinity for MTs(*22*) (ref. 22 describes a weak *in cell* activity as well). It is

known that taxanes bind with high affinity to assembled s-tubulin(*23*) while having undetectable affinity for unassembled c-tubulin(*4*). We found that baccatin III shows a detectable affinity ($Kb_{25°C}$ 3.0±0.5x10^3 M^{-1}) to unassembled c-tubulin (**Fig. 3C**), in the same range as the ones previously measured for other compounds able to bind and co-crystallize with tubulin, such as epothilone A 0.8±0.3×10^4 M^{-1} (*24*) and discodermolide 2.0±0.7×10^4 M^{-1} (*25*). Therefore, we hypothesized that the presence of the C13 side chain of the taxanes aforementioned might preclude the binding to the c-tubulin form present in both the T_2R-TTL and the TD1 complexes. Subsequently, we obtained a T_2R-TTL-baccatin III complex structure at 1.9Å resolution (**Fig. 2A, Fig. S1A & D, Table S1**) (PDB ID 7A7I) and found that baccatin III binds to the taxane site with its C2-benzoyloxy ring C stacked between the side chains of βH229 and βL275 in the leucine rich pocket formed by the side chains of βC213, βL217, βL219, βD226, βH229, βL230 and βL275. Its carbonyl oxygen forms a weak hydrogen bond to the main chain amide of βR278 (**Fig. 2A**). The C10 acetate is exposed to the solvent and together with the C12 methyl is in Van der Waals distance to βG370 of the βS9-βS10 loop. Furthermore, the oxetane oxygen and the C13 hydroxyl form hydrogen bonds to the main chain amide of βT276 and to βH229 NE2, respectively. The C4 acetate is buried in the hydrophobic pocket formed by βL230, βA233, βF272, βP274, βL275, βM302, βL371 and the aliphatic portion of the βR369 side chain. Strikingly, we only found well-defined electron density for the amino-terminal section of the βM-loop up to βR278, while the remaining portion of the βM-loop was disordered. This suggests that baccatin III does not promote the stabilization of this region into a helical conformation, in contrast to what has been previously observed for both the taxane-site binders zampanolide and epothilone A(*12*).

Aiming to understand the implication of Ptx's C13 ring A moiety (or its equivalent tert-butyl in Dcx) on tubulin activation and to understand why it precludes binding to c-tubulin, we took a synthetic effort to obtain new taxane ligands with modified side chains able to crystallize in complex with c-tubulin. We produced a series of modified taxanes bearing smaller groups at the ring A position of Ptx: acrylamide (**2a**), haloacetamide (**2b, 2c**) and isocyanate (**2d**) (**Fig 1C**). Since we measured binding affinity of **2a** to unassembled tubulin dimers ($Kb_{25°C}$ 0.8±0.3x10^3 M^{-1}) (**Fig. 3C),** but not of N-AB-PT(*15*), Chitax 40(*16*) or Chitax 68(*17*), we concluded that the new modification applied to the Ptx structure increases the binding of the compounds for the unassembled c-tubulin. In fact, we unequivocally found difference electron densities at the taxane sites of T_2R-TTL

crystals soaked with **2a** (**Fig S1B, E**) (PDB ID 7A7F) and **2b** (**Fig S1C, F**) (PDB ID 7A7J). The corresponding structures were refined to 1.95 Å and 2.35 Å resolution, respectively. Although these densities displayed continuity between the 3'-N moieties of these ligands and the side chain of βH229, covalent adduct formation was discarded both biochemically **(see extended data)** and crystallographically with the help of anomalous data collected from a T_2R-TTL-**2b** crystal at the bromine peak wavelength (0.91501 Å, **Fig S1G**).

The structure showed that compound **2a** forms comparable interactions with both the C2-benzoyloxy ring C and the oxetane moieties as described for baccatin III (**Fig. 2B,C**). However, the core ring is tilted towards helix βH6 and strand βS7 by 18.5˚ (angle between the two C1-C9 axis**;** $rmsd_{bacIII-2a}$ of 0.794 Å for 39 core atoms), adopting a pose that is closer to that observed for Ptx bound to s-tubulin (PDB ID 6WVR; $rmsd_{2a-Ptx}$ of 0.845 Å for 56 core atoms **Fig. 4B;** $rmsd_{bacIII-Ptx}$ of 1.048 Å for 42 core atoms **Fig. 4B**). Similar to Ptx bound to s-tubulin, the C39 carbonyl of the C13-3'-N-acrylamide moiety of **2a** forms an equivalent hydrogen bond to the NE2 of βH229 (**Fig. 2B, 4B**). The acetamide moiety is exposed to the solvent and forms water-mediated hydrogen bonds to the side chains of βE22 and βR369, a space that is otherwise occupied by water molecules in the baccatin III structure. In the context of Ptx-bound MTs the 3'-N-benzamido phenyl ring A moiety of Ptx occupies this space and the βD26 side chain replaces the βR369 side chain, which adopts a flipped-out conformation (PDB ID 6WVR, **Fig. 2B, Fig. 4B**). The absence of the C10 acetate in **2a** compared to baccatin III has no impact on the orientations and conformations of both the βS9-βS10 and the βM-loops, which are closely similar in both structures (**Fig. 2C**). In both structures, we found the βT5-loops in the "out" conformation.

Interestingly, we found that the replacement of ring A by an acrylamide moiety has a deep impact in the compound's activity showing a four orders of magnitude lower cytotoxicity than Ptx in KB and HeLa tumoral cells (**Table 1**). Biochemically **2a** and **2b** behaved as weaker assembly inducers compared to Ptx (PEDTA buffer, **Fig. 3AB**). Because both the tubulin assembly induction power and the cytotoxicity of MT stabilizing agents is strongly linked to the binding affinity for MTs(*13, 23, 26*) we expected a strongly compromised ability to bind MTs for **2a** and **2b**. Surprisingly, that was not the case and the binding constants of **2a** ($0.46 \pm 0.06 \times 10^7$ M^{-1}) and **2b** ($0.32 \pm 0.03 \times 10^7$ M^{-1}) to MTs were similar to the one observed for Ptx ($1.43 \pm 0.17 \times 10^7$ M^{-1} (*23*)). Furthermore,

also baccatin III (inactive compound) displayed a significant binding affinity for assembled MTs $1.5x10^5 M^{-1}$ (*22*), which is even higher than that of other taxanes with detectable activity(*16*). Therefore, we concluded that the increase of binding affinity for the curved conformation (and the subsequently reduction of the preferential binding for the straight one) could be linked to decreased MT stabilizing activity and cytotoxicity.

Ptx binds to the straight conformation of unassembled tubulin in solution.

To obtain information about the transient Ptx/unassembled tubulin interactions in solution we approached TR-NOESY experiments. Surprisingly, despite both the low solubility of Ptx and the reported very low binding constant of Ptx to unassembled, c-tubulin ($< 10^3$ M^{-1})(*4*), we found weak but clear signals in the spectra (**Fig. 5C**). In the presence of MTs, the spectra displayed strong signals (**Fig. 5D**), as expected(*25*). As a control we acquired the NOESY spectrum of Ptx in the absence of tubulin, no peaks were detected (not shown) indicating that all the signals observed in the presence of tubulin are TR-NOESY ones. Strikingly, the correlation between both spectra was almost perfect (the observed displacement in the position of the cross peaks is due to the different temperature at which the spectra were recorded 298 K for unassembled tubulin vs 310 K for MTs), suggesting that the conformation of Ptx was similar when bound to unassembled, c-tubulin (Kb $< 10^3$ M^{-1}) or assembled s-tubulin (Kb 10^7 M^{-1})(*23*). Instead, previous studies with epothilone and discodermolide revealed differences on the bound conformation depending on the tubulin assembly state(*24, 25*). The quantitative analysis of the TR-NOESY spectra (Table S2), indicates that the conformation adopted by Ptx in solution (**Fig. 5A**) is nearly coincident with this determined by cryo-EM. Considering that Ptx binding to unassembled, c-tubulin is not detected either by biochemical methods nor by macromolecular crystallography, we assumed that the equal conformation of Ptx bound to assembled and unassembled tubulin could be attributed to the observation of Ptx bound to a small fraction of s-tubulin (**see discussion and extended discussion**).

To further characterize the ligand binding epitope and to probe the pharmacophore region of Ptx bound to tubulin, we acquired STD-NMR spectra of tubulin preparations obtained under unassembled and assembled conditions. Similar to what has been described for Dcx(*25*), we found STD signals under both studied conditions (assembled and unassembled tubulin with very similar profiles **(Fig. S3)**, denoting a similar binding mode of Ptx under both conditions. However, experiments performed with **2a** under

unassembled and assembled tubulin conditions **(Fig. S4)** showed subtle differences in the C13 side chain section corresponding to the acrylamide moiety that replaces the aromatic ring A in Ptx, thereby suggesting two distinct interaction patterns of this moiety depending on the tubulin conformation. Additionally, similar STD profiles of baccatin III bound to unassembled and assembled tubulin **(Fig. S5)** were found, as expected, because this compound lacks the C13 side chain responsible for the differential interaction for c- and s-tubulin. Together, these results support that the weak signals of Ptx bound to unassembled tubulin arise from the compound bound to the small proportion of unassembled s-tubulin in equilibrium with c-tubulin.

C13 side chain promoted perturbations in unassembled c-tubulin, strengthen on straight MTs.

To understand the contribution of the C13 side chain to the observed differences in biochemical and biological activity and in the NMR-experiments, we further investigated the perturbations induced by binding of baccatin III and **2a** to the unassembled c-tubulin β chains. To this aim, we first superimposed the structures of apo (PDB ID 4I55), baccatin III and **2a** bound states onto the N-terminal β-sheets of β-tubulin (residues 3-9, 63-66, 132-138, 163-169 and 198-202; $rmsd_{BacIII}$ 0.08 Å of 29 C_α; $rmsd_{\mathbf{2a}}$ 0.10 Å of 29 C_α) and calculated the rmsd-differences between both the apo and the taxane bound states using the rmsdByRes function in PyMOL (**Fig. 6B, D**). The rmsd-differences were also plotted and mapped onto the corresponding structures to highlight the major regions of perturbation (**Fig. 6A, C**). Comparable perturbations were observed for backbone and all atoms in the helix βH2', the βT5-loop, the βM-loop basis, the helix βH9, and both the helix βH11-βH11' and βH12 regions of both the ligands, while the rmsd-values for both the βS2'-βS2" and the βS9-βS10 loops were higher for **2a**. To investigate the effect of the observed perturbations on the relative domain arrangements in β-tubulin of the individual complexes, we further superimposed the β-tubulin chains onto their central helices βH7. For baccatin III, a mild relative twist between the N-terminal and the intermediate domains was observed (**Fig. S2**; **Suppl. Movie M1, M2**), while binding of **2a** rather caused both the N-terminal and intermediate domains of the β-tubulin molecule to slightly move apart (**Fig. S2; Suppl. Movie M3, M4**).

Since these subtle movements were observed in the c-tubulin conformations in the context of a crystal lattice, we sought to compare them to the perturbations that occur upon Ptx binding in the context of MTs. To this aim, we performed the same type of analysis by superimposing the N-terminal β-sheets of β-tubulin from the cryo-EM reconstruction of Ptx-bound GDP-MTs (PDB ID 6WVR)(*27*) onto the corresponding domains of the undecorated apo GDP-MT structure (PDB ID 6DPV; rmsd 0.304 Å 30 C_α)(*28*). The rmsd-analysis of Ptx bound MTs revealed comparable but more pronounced perturbations to the ones observed for **2a** for the βS2'-S2", the βH3, the βS9-βS10 and the βH11-βH12 regions, with a more prominent effect on the βM-loop (**Fig. 4C, D**). These observations suggested that perturbations induced by the C13 side chain may have an impact on stabilizing the MT-lattice, since they occur at positions that contribute to lateral contacts in MTs, which is in agreement with the results published by Debs and co-workers(*27*), where Ptx-bound MTs displayed higher curvature and distinct βM-loop movements.

C13 side chain is not required for lattice expansion but affects lateral contacts in MTs.

The main structural effect of Ptx on the MT lattice is a longitudinal expansion that have been related to the stabilization effect of this compound(*29, 30*). We have previously validated X-ray fiber diffraction of shear-flow aligned MTs as an accurate technique to discern main MT lattice structural features(*31, 32*) and, we used it to elucidate how our Ptx derivatives with reduced activities affect the structure of MTs.

The meridional diffraction patterns are related to axial helical repetitions on the MT lattice and show a layer line at 4 nm (**Fig. 7**) and, when the lattice is expanded, a second weaker layer line at 8 nm due to the length differences between α- and β- tubulin(*31*). Additionally, the position of the 1 nm layer line (4^{th} harmonic of the 4 nm layer line) also moves towards the center of the image when lattice expansion occurs. Both, Ptx (**Fig. 7A**) and Dcx (**Fig. 7B**) induced MTs expansion, as expected(*29*). And this expansion occurred in either case, when the addition of the drug was previous to assembly into MT using GTP-bound or GDP-bound tubulin (named "pre-" in **Table S3**) or when added directly to assembled MTs (named "post-" in **Table S3**). This was in clear opposition to previous observations in which expansion was only observed in pre-addition experiments(*10*). Interestingly, **2a** (**Fig. 7C**), **2b** (**Fig. 7D**) and baccatin III

(**Fig. 7E**) showed similar MT expanded lattices indicating that the lattice expansion is not related with taxane's MT stabilizing activity. Note that the diffraction patterns of MTs stabilized with **2a** or **2b** showed a diffuse 1 nm layer line showing variations on the monomer rise, which is in clear contrast to all other analyzed taxanes that displayed a sharp band (i.e., a fixed monomer rise). Furthermore, we found that the effect of these compounds on the lateral interactions (equatorial diffraction patterns) differed and, thereby variations in the C13 side chain might modulate the lateral interactions between PFs (**Table S3**).

Discussion

Previous studies of MT stabilization by Ptx controversially discussed the interaction of the drug with the βM-loop and lattice effects, through lateral versus longitudinal contacts(*10, 29, 33*) and communication between β-tubulin domains through core helix βH7(*34*). Here, we undertook a unifying approach to discern which parts of the Ptx molecule are involved in protein recognition, in inducing conformational changes on tubulin and MT and, in its final stabilization activity. We have studied and compared the structural effects as well as the biochemical and cellular activity of the Ptx core region, baccatin III, and of two engineered Ptx derivatives, **2a** and **2b,** with modifications at the C13 side tail affecting ring A. We have gained insight into our understanding of the molecular mechanism of action of Ptx finding that: (i) the taxane core (baccatin III) is responsible for most of the interacting energy of Ptx but it is only marginally involved in the stabilization activity, (ii) the bulky hydrophobic group at 3'-N of the C13 side tail distinguishes the s- from the c-tubulin conformation and promotes stabilization, and, (iii) the lattice expansion is unrelated to the MT stabilization mechanism of Ptx.

The high-resolution crystallographic data show that the taxane core region reduces the flexibility of the M-loop by inducing a partial structuring of its N-terminal section. Further changes occur in the presence of a C13 side chain (**2a** and **2b**), tilting the positioning of the Ptx core region by 18.5º within the pocket, and inducing a subtle reorientation of the tubulin domains. Therefore, tubulin conformational changes related to the binding of taxanes are initiated when bound to c-tubulin (in solution or at the tip of MTs(*35*)) and strengthen upon tubulin straightening through the formation of polymer contacts. Despite we have not observed a complete folding of the βM-loop upon baccatin

III, **2a** and **2b** binding, perturbations were detected in the c-tubulin structures, which were comparable but weaker to the ones observed upon Ptx-binding to assembled MTs. Moreover, fiber diffraction studies showed differences on the lateral arrangement of shear-flow aligned MTs bound to these compounds. This suggests that Ptx and Ptx-derived compounds indeed lock the lateral contacts to promote MT lattice stability through interactions with the N-terminal section of the βM-loop, which is in agreement with both the observations reported by Manka and Moores(*33*) and by Debs and co-workers(*27*). Interestingly, fiber diffraction studies also showed the same MT-lattice expansion for these analogs as the one observed in the presence of the active compounds Ptx and Dcx. This structural feature is not related to the stabilization power since all taxanes and Ptx-derived compounds similarly induced MT axial expansion but their stabilization power ranged from highly stabilized MTs (Ptx and Dcx) to lower (**2a**) or none or very weak (bacattin III). Therefore, the axial effect of these taxanes and hence, the longitudinal contacts might not be the main reason of the stabilizing activity and this activity may rely more on the effect of these compounds on the lateral interactions.

Importantly, the Ptx structure is optimized for its activity and changes introduced at the ring A of the C13 side chain severely hamper the MT stabilizing activity. These changes did not affect the binding to s-tubulin in MTs since the binding modes of **2a** and **2b** were very similar to the ones described for Ptx-bound to MTs(*10, 29, 33*) (**Fig. S6**), but significantly enhanced the interaction with unassembled c-tubulin. The curved-to-straight conformational change in tubulin induces subtle modifications at the taxane-site that were also previously detected by changes of the STD profiles of other taxane site binders (discodermolide and epothilones)(*24, 25*). In contrast, no changes in the STD profiles were detected for Ptx samples. Moreover, TR-NOESY determined, Ptx-bound conformations in unassembled tubulin and MTs were identical (**Figs 5; S3; S4; S5**) (detailed information about the conformational studies are given in supporting information, including the quantitative analysis of the NOE intensities by taking into account the full matrix relaxation treatment implemented in MSpin software(*36*)). We hypothesize that very likely we are detecting the binding of Ptx to a small fraction of unassembled, s-tubulin. This binding event would shift the equilibrium towards the straight conformation due to the higher affinity **(Fig. 8, extended discussion)** and hence, Ptx-bound unassembled s-tubulin would easily nucleate and would be more prone to assembly because the energy needed for the curved-to-straight transition is provided by

Ptx binding **(extended discussion)**. Furthermore, these nucleated, straight oligomers (previously observed in(*37*)) would be less prone to disassembly. In the case of assembled MTs, the effect of the preferential binding implies that drug-bound subunits would be restricted to bend (bending would require release of the tightly bound drug), therefore preserving the stabilizing contacts. Concordantly, compounds with higher differential affinity between c- vs s-tubulin conformations (Ptx and Dcx) are better assembly inducers and more cytotoxic than those with lower difference of affinities (Ptx derivatives of this work) (**Fig. 3** and **Table 1**), supporting a link between preferential binding for the s-tubulin conformation and the stabilizing activity.

We have seen that several secondary structural elements are perturbed upon Ptx derivative binding. Moreover, we observed a major structural difference in proximity of the position occupied by the 3'-N-benzamido phenyl ring A moiety of Ptx in MTs: In the c-tubulin-**2a** structure**,** the βR369 side chain occupies the same space as the βD26 side chain in the context of the s-tubulin conformation in MTs. These changes could explain the observed differences of binding affinity for the unassembled and the assembled tubulin structures. The C13 side chain is involved in the interaction with helix βH1, which is flanked by the βH1-βS2 loop (the lock in the key-lock lateral interplay with the βM-loop). Upon transition to the assembled s-tubulin state, this space is narrowed down by the side chains of βD26, βK19, βE22 and βH229 to form a favorable environment for the interaction with the ring A moiety, which may lock the Ptx-bound tubulin in the straight conformation (**Fig. 9B**). In the absence of the C13 side chain (baccatin III) or in the presence of the less bulky moieties in ring A position (**2a** and **2b**), ligand binding is likely less affected by the conformational transition from curved to straight, since much looser interactions can still be established to the charged residue side chains of the βS9-βS10 loop and the helix H1 through water molecules (**Fig. 2C, Fig. 9A**). However, they may not be strong enough to lock the tubulin in the straight conformation. These observations suggest that modifications of the C13 side chain greatly affect the differential binding affinity of Ptx derived taxanes for unassembled c- vs. assembled s-tubulin in MTs.

In summary, our results support the essential role of the ring A in C13 side chain of Ptx in the mechanisms of MT stabilization. The presence of the ring A in the side chain precludes binding to c-tubulin and contributes to the consolidation of lateral contacts over the axial ones.

Materials and Methods

Proteins and ligands

Purified calf brain tubulin and chemicals were obtained as previously described(*4, 38*). Paclitaxel (Taxol®) (Ptx) was from Alfa Aesar Chemical, Docetaxel (Taxotere®) (Dcx) was kindly provided by Rhône Poulenc Rorer, Aventis (Schiltigheim, France), baccatin III was from Sigma, Flutax-2, Chitax 40, 3'N-aminopaclitaxel (N-AB-PT) and Chitax-68 were synthesized as described(*15-17, 39*). All compounds were diluted in 99.8% D6-DMSO (Merck) to a final concentration of 20 mM and stored at -20 ºC. Their solubility in aqueous media was determined as described in(*40*), Flutax-2 was found soluble, while a 100 µM solubility was found for docetaxel and a 50 µM for both paclitaxel and Chitax40.

Biochemistry and cell biology

HeLa S3 and HeLa βIII(*41*) cells were cultured in Dulbecco Modified Eagle Medium (DMEM) supplemented with 10% fetal calf serum (FCS), glutamine (2 mM), gentamycin (40 µg/mL), penicillin (100 IU/mL), and streptomycin (100 µg/mL). The medium for HeLa βIII cells was additionally supplemented with geneticin (0.5 mg/mL). KB-3-1 (HeLa cells) derived from a cervical carcinoma and its multidrug resistant counterpart KB-V1 (*42*) were grown in DMEM, 10% FCS, 1 mM piruvate and penicillin (50 IU/mL) streptomycin (50 mg/mL), the latter cell line with 1 mg/mL of vinblastine. Compounds were screened for toxicity against HeLa cells (KB-3-1, KB-V1, HeLa S3 and HeLa βIII) using MTT assay following previously described protocols with minor modifications(*43*). Briefly, cells were seeded in 96-well plates using regular DMEM medium and incubated for 24 h. Then, cells were treated with vehicle or compound diluted in the DMEM medium without serum for 72 h. The vehicle and compound solution was changed once every 24 h. MTT solution (5 mg/ml) was added into each well and further incubated for another 2 h. Finally, DMSO was added to stop the MTT reaction and then, optical density was measured at 570 nm using a Molecular Devices SpectraMax M5 (Molecular Devices, USA). The statistical significance of differences in IC_{50} values were evaluated using the t-test option implemented in the Sigma Plot 13 software package (version 13, Systat Software, Inc., San Jose, CA, USA).

Polymerization of 20 μM Tubulin in PEDTA buffer (10 mM sodium phosphate (NaPi), 1 mM EDTA, 1 mM GTP, pH 6.7) plus 4 or 7 mM $MgCl_2$, was monitored in the presence of 25 μM taxanes by turbidity at 350 nm employing a Thermo Appliskan plate reader (Thermo Fisher, Waltham, MA, USA). The binding constants of the compounds to the taxane binding site of stabilized cross-linked microtubules (MTs) were measured by Flutax-2 displacement as previously described(*23*).

The binding constants of both **2a** and baccatin III to unassembled dimeric tubulin were measured by centrifugation. Increasing amounts of dimeric tubulin (up to 150 μM) prepared in NaPi-GTP buffer (10 mM sodium phosphate, 0.1 mM GTP, pH 7.0) were incubated with a fixed concentration (50 μM) of either baccatin III or **2a**, incubated for 30 min at 25 ºC and centrifuged at 100000 rpm in a TLA-100.2 rotor for 2h at 25 ºC. Then, samples were divided into upper (100 μL) and lower (100 μL) parts and 100 μL of NaPi were added to both of them. Afterwards, 10 μM of either docetaxel or paclitaxel were added as internal standard and samples were subjected three times to an organic extraction using dichloromethane (v:v). Dichloromethane was removed by evaporation and samples were resuspended in methanol 70%. Finally, ligand content was analyzed using an HPLC system (Agilent 1100 Series) and samples were separated using a Zorbax Eclipse XDB-C18 column (Methanol 70% isocratic condition; 20 minutes runs). Tubulin content was determined by BCA for each sample. Ligand concentration in the upper 100 μL was considered as free concentration, while this in the lower 100 μL was considered as the sum of bound and free concentrations. Binding constants of tubulin for the ligand were calculated assuming a single binding site per tubulin dimer using SIGMAPLOT 14.5 Sigmastat Software Inc.

Binding constant of **2a** to cross-linked assembled MTs was measured as previously described(*16*).

Reactivity of **2a** with tubulin and MTs was studied using organic solvent extraction and HPLC. Reaction of the compound with MTs was studied by incubating 25 μM of tubulin in 10 mM NaPi, 1mM EDTA, 0.1 mM GTP and 7 mM $MgCl_2$ buffer pH 6.7, in the presence of 27.5 μM of **2a** (polymerizing conditions). Duplicated samples were collected from the reaction tube at 0', 30', 1h, 2h and 4h and were centrifuged at 50000 rpm in a TLA100.2 rotor for 20'. Subsequently, supernatant was collected and a similar volume of buffer was used to dissolve the pellet. Paclitaxel at 10 μM was added to all the

samples as internal standard. Duplicated samples were subjected to organic solvent extraction either with 3 times of dichloromethane (v:v) or with the milder solvent ethyl acetate, and the organic solvent was evaporated afterwards. Residues left were resuspended in 70% methanol/Water and developed isocratically using an Agilent 1100 HPLC system connected to a reverse phase column Zorbax Eclipse XDB-C18 (mobile phase 70% methanol) with detection at 254 and 273 nm to quantify **2a** using the internal standard.

Reaction of **2a** with dimeric tubulin was also studied. 20 μM tubulin in 10 mM NaPi, 1 mM EDTA, 0.1 mM GTP buffer pH 7.0 (non-polymerizing conditions) was incubated for 2 hours with 22.5 μM of **2a** at 4°C and 37°C, after incubation 10 μM of paclitaxel was added to all the samples as internal standard. Samples were further developed and analyzed as described above. As control, a sample of **2a** in the absence of tubulin was processed and analyzed in the same way.

NMR sample preparation and experiments

Samples of ligand bound to non-polymerized α/β–tubulin -heterodimers were prepared in 3 mm NMR tubes using a 300 μM concentration of baccatin III or 150 μM of paclitaxel and 10 μM of tubulin in D_2O (10 mM NaPi, 0.1 mM GTP pD 7.3) as described in(*25*). Samples of ligands bound to MTs were prepared in 3 mm NMR tubes using a 150 μM of paclitaxel and 20 μM of tubulin in D_2O (10 mM KPi, 0.1 mM GMPCPP, 6 mM $MgCl_2$, pD 7.0) as described in(*25*). An 8% DMSO was added to the buffer to solubilize the ligand. NMR spectra were then recorded at 298 K (dimeric tubulin samples) or 310 K (polymeric tubulin samples) in D_2O on a Bruker AVANCE 500 MHz or on a 700 MHz spectrometer equipped with a triple-channel cryoprobe as described in(*25*). Additionally, the oligomerization state of the tubulin samples for the NMR experiments was analyzed by sedimentation velocity in a Beckman Optima XL-I analytical ultracentrifuge as described(*25*).

Crystallization, Data Collection and Structure Determination

Crystals of T_2R-TTL were generated as described(*12, 14*). Suitable T_2R-TTL crystals were soaked for 8h in reservoir solutions (2-4% PEG 4K, 2-10% glycerol, 30 mM $MgCl_2$, 30 mM $CaCl_2$, 0.1 M MES/Imidazole pH 6.7) containing either 10 mM

baccatin III, 5 mM **2a** or **2b.** Ssubsequently, crystals were flash cooled in liquid nitrogen following a brief transfer into cryo solutions containing the reservoir supplemented with 16% and 20% glycerol. All data were collected at beamline X06DA at the Swiss Light Source (Paul Scherrer Institut, Villigen, Switzerland). Images were indexed and processed using XDS(*44*). Structure solution using the difference Fourier method and refinement were performed using PHENIX(*45*). Model building was carried out iteratively using the Coot software(*46*). Data collection and refinement statistics for all three T_2R-TTL-complexes are given in Supplemental Table S1. Molecular graphics and analyses were performed with PyMol (The PyMOL Molecular Graphics System, Version 2.3.2, Schrödinger, LLC). To compare the structures of both baccatin III and **2a** complexes in the curved tubulin (c-tubulin) conformation to the straight tubulin (s-tubulin) in paclitaxel stabilized MT (PDB ID 5SYF), all structures were superimposed onto the taxane-site of **2a** (residues 208-219+225-237+318-320+359-376+272-276+287-296; $rmsd_{BacIII}$ 0.171 Å (48 C_α atoms), $rmsd_{5SYF}$ 0.868 Å (52 C_α atoms)).

MT shear-flow alignment and X-ray fiber diffraction experiments

X-ray fiber diffraction data were collected in BL11-NDC-SWEET beamline of ALBA Synchrotron at a λ=0.827 nm as described in(*32*). Radial structural parameters (MT diameter and average inter-PT distances) and dimer/monomer length (from the 4th harmonic of the first layer-line signals) were determined as described in(*32*).

References

1. M. W. Saville *et al.*, Treatment of HIV-associated Kaposi's sarcoma with paclitaxel. *The Lancet* **346**, 26-28 (1995).
2. J. J. Field, J. F. Diaz, J. H. Miller, The Binding Sites of Microtubule-Stabilizing Agents. *Chemistry & Biology* **20**, 301-315 (2013).
3. P. B. Schiff, S. B. Horwitz, Taxol assembles tubulin in the absence of exogenous guanosine 5'-triphosphate or microtubule-associated proteins. *Biochemistry* **20**, 3247-3252 (1981).
4. J. F. Díaz, M. Menéndez, J. M. Andreu, Thermodynamics of ligand-induced assembly of tubulin. *Biochemistry* **32**, 10067-10077 (1993).
5. E. Nogales, S. G. Wolf, K. H. Downing, Structure of the alpha beta tubulin dimer by electron crystallography. *Nature* **391**, 199-203 (1998).
6. E. Nogales, M. Whittaker, R. A. Milligan, K. H. Downing, High-resolution model of the microtubule. *Cell* **96**, 79-88 (1999).

7. B. Gigant *et al.*, The 4 A X-ray structure of a tubulin:stathmin-like domain complex. *Cell* **102**, 809-816 (2000).
8. L. Pecqueur *et al.*, A designed ankyrin repeat protein selected to bind to tubulin caps the microtubule plus end. *Proc Natl Acad Sci U S A* **109**, 12011-12016 (2012).
9. A. E. Prota *et al.*, Structural Basis of Microtubule Stabilization by Discodermolide. *Chembiochem* **18**, 905-909 (2017).
10. E. H. Kellogg *et al.*, Insights into the Distinct Mechanisms of Action of Taxane and Non-Taxane Microtubule Stabilizers from Cryo-EM Structures. *J Mol Biol* **429**, 633-646 (2017).
11. F. A. Balaguer *et al.*, Crystal Structure of the Cyclostreptin-Tubulin Adduct: Implications for Tubulin Activation by Taxane-Site Ligands. *Int J Mol Sci* **20**, (2019).
12. A. E. Prota *et al.*, Molecular mechanism of action of microtubule-stabilizing anticancer agents. *Science* **339**, 587-590 (2013).
13. C. Trigili *et al.*, Structural Determinants of the Dictyostatin Chemotype for Tubulin Binding Affinity and Antitumor Activity Against Taxane- and Epothilone-Resistant Cancer Cells. *ACS Omega* **1**, 1192-1204 (2016).
14. A. E. Prota *et al.*, Structural basis of tubulin tyrosination by tubulin tyrosine ligase. *J Cell Biol* **200**, 259-270 (2013).
15. Y. Li, R. Edsall, Jr., P. G. Jagtap, D. G. Kingston, S. Bane, Equilibrium studies of a fluorescent paclitaxel derivative binding to microtubules. *Biochemistry* **39**, 616-623 (2000).
16. R. Matesanz *et al.*, Optimization of taxane binding to microtubules. Binding affinity decomposition and incremental construction of a high-affinity analogue of paclitaxel. *Chem Biol* **15**, 573-585 (2008).
17. Y.-T. Ma *et al.*, A Series of Enthalpically Optimized Docetaxel Analogues Exhibiting Enhanced Antitumor Activity and Water Solubility. *Journal of Natural Products* **81**, 524-533 (2018).
18. G. Samaranayake, K. A. Neidigh, D. G. I. Kingston, Modified Taxols, 8. Deacylation and Reacylation of Baccatin III. *Journal of Natural Products* **56**, 884-898 (1993).
19. J. Parness, D. G. I. Kingston, R. G. Powell, C. Harracksingh, S. B. Horwitz, Structure-activity study of cytotoxicity and microtubule assembly in vitro by taxol and related taxanes. *Biochemical and Biophysical Research Communications* **105**, 1082-1089 (1982).
20. H. Lataste, V. Senilh, M. Wright, D. Guénard, P. Potier, Relationships between the structures of taxol and baccatine III derivatives and their in vitro action on the disassembly of mammalian brain and Physarum amoebal microtubules. *Proceedings of the National Academy of Sciences* **81**, 4090-4094 (1984).
21. D. G. Kingston, Recent advances in the chemistry of taxol. *J Nat Prod* **63**, 726-734 (2000).
22. J. M. Andreu, I. Barasoain, The interaction of baccatin III with the taxol binding site of microtubules determined by a homogeneous assay with fluorescent taxoid. *Biochemistry* **40**, 11975-11984 (2001).
23. R. M. Buey *et al.*, Microtubule interactions with chemically diverse stabilizing agents: Thermodynamics of binding to the paclitaxel site predicts cytotoxicity. *Chem. Biol.* **12**, 1269-1279 (2005).

24. A. Canales *et al.*, Molecular recognition of epothilones by microtubules and tubulin dimers revealed by biochemical and NMR approaches. *ACS Chem Biol* **9**, 1033-1043 (2014).
25. A. Canales *et al.*, Insights into the interaction of discodermolide and docetaxel with dimeric tubulin. Mapping the binding sites of microtubule-stabilizing agents using an integrated NMR and computational approach. *ACS Chem. Biol.* **6**, 789-799 (2011).
26. R. M. Buey *et al.*, Interaction of Epothilone Analogs with the Paclitaxel Binding Site; Relationship between Binding Affinity, Microtubule Stabilization, and Cytotoxicity. *Chem Biol* **11**, 225-236 (2004).
27. G. E. Debs, M. Cha, X. Liu, A. R. Huehn, C. V. Sindelar, Dynamic and asymmetric fluctuations in the microtubule wall captured by high-resolution cryoelectron microscopy. *Proceedings of the National Academy of Sciences* **117**, 16976-16984 (2020).
28. R. Zhang, B. LaFrance, E. Nogales, Separating the effects of nucleotide and EB binding on microtubule structure. *Proc. Natl. Acad. Sci. USA* **115**, E6191-E6200 (2018).
29. Gregory M. Alushin *et al.*, High-Resolution Microtubule Structures Reveal the Structural Transitions in αβ-Tubulin upon GTP Hydrolysis. *Cell* **157**, 1117-1129 (2014).
30. A. Rai *et al.*, Taxanes convert regions of perturbed microtubule growth into rescue sites. *Nature Materials* **19**, 355-365 (2020).
31. S. Kamimura, Y. Fujita, Y. Wada, T. Yagi, H. Iwamoto, X-ray fiber diffraction analysis shows dynamic changes in axial tubulin repeats in native microtubules depending on paclitaxel content, temperature and GTP-hydrolysis. *Cytoskeleton* **73**, 131-144 (2016).
32. J. Estevez-Gallego *et al.*, Structural model for differential cap maturation at growing microtubule ends. *Elife* **9**, (2020).
33. S. W. Manka, C. A. Moores, The role of tubulin-tubulin lattice contacts in the mechanism of microtubule dynamic instability. *Nat Struct Mol Biol* **25**, 607-615 (2018).
34. L. A. Amos, J. Lowe, How Taxol stabilises microtubule structure. *Chem Biol* **6**, R65-69 (1999).
35. J. R. McIntosh *et al.*, Microtubules grow by the addition of bent guanosine triphosphate tubulin to the tips of curved protofilaments. *The Journal of Cell Biology* **217**, 2691 (2018).
36. A. Navarro-Vázquez, MSpin-RDC. A program for the use of residual dipolar couplings for structure elucidation of small molecules. *Magnetic Resonance in Chemistry* **50**, S73-S79 (2012).
37. C. Elie-Caille *et al.*, Straight GDP-tubulin protofilaments form in the presence of taxol. *Curr Biol* **17**, 1765-1770 (2007).
38. J. M. Andreu, in *Methods Mol. Biol.,* J. Zhou, Ed. (Humana Press Inc., Totowa, NJ, 2007), vol. 137, chap. Microtubule Protocols, pp. 17-28.
39. J. F. Diaz, R. Strobe, Y. Engelborghs, A. A. Souto, J. M. Andreu, Molecular recognition of taxol by microtubules. Kinetics and thermodynamics of binding of fluorescent taxol derivatives to an exposed site. *J Biol Chem* **275**, 26265-26276 (2000).
40. G. Saez-Calvo *et al.*, Triazolopyrimidines Are Microtubule-Stabilizing Agents that Bind the Vinca Inhibitor Site of Tubulin. *Cell Chem Biol* **24**, 737-750 e736 (2017).

41. P. A. Joe, A. Banerjee, R. F. Luduena, The roles of cys124 and ser239 in the functional properties of human betaIII tubulin. *Cell Motil Cytoskeleton* **65**, 476-486 (2008).
42. D. W. Shen *et al.*, Multiple drug-resistant human KB carcinoma cells independently selected for high-level resistance to colchicine, adriamycin, or vinblastine show changes in expression of specific proteins. *Journal of Biological Chemistry* **261**, 7762-7770 (1986).
43. Y. Yang *et al.*, H6, a novel hederagenin derivative, reverses multidrug resistance in vitro and in vivo. *Toxicology and Applied Pharmacology* **341**, 98-105 (2018).
44. W. Kabsch, XDS. *Acta Crystallogr. Sect. D* **66**, 125-132 (2010).
45. P. D. Adams *et al.*, PHENIX: a Comprehensive Python-based System for Macromolecular Structure Solution. *Acta Crystallogr. Sect. D* **66**, 213-221 (2010).
46. P. Emsley, B. Lohkamp, W. G. Scott, K. Cowtan, Features and development of Coot. *Acta Crystallogr D Biol Crystallogr* **66**, 486-501 (2010).
47. Y. Tang *et al.*, Modification of C-seco taxoids through ring tethering and substituent replacement leading to effective agents against tumor drug resistance mediated by betaIII-Tubulin and P-glycoprotein (P-gp) overexpressions. *Eur J Med Chem* **137**, 488-503 (2017).

Acknowledgments

We thank Ganadería Fernando Díaz for calf brains supply and staff of beamlines X06DA of the Swiss Light Source (Paul Scherrer Institut, Villigen PSI, Switzerland) and BL11-NDC-SWEET (ALBA, Cerdanyola del Vallès, Spain) for their support. We also thank Mr. Pedro Gascón Blanco for his private donation to the project to support a month of a student salary.

This article is dedicated to the memory of Dr. Linda Amos, a dear friend and pioneer in the study of microtubules and the mechanism of action of Taxol(*34*), who passed away while we were assembling this manuscript.

Funding: Ministerio de Ciencia e Innovación PID2019-104545RB-I00 (J.F.D.); CSIC PIE 201920E111 (J.F.D.); CSIC PIE 202020E301(J.F.D.); Fondo de Investigaciones Sanitarias COV20/01007 (J.F.D.); EU H2020-MSCA-ITN-2019 860070 TUBINTRAIN (J.F.D. , A.E.P.); Swiss National Science Foundation (31003A_166608) (M.O.S.) ; JSPS KAKENHI (16K07328/17H03668) to (S.K.); NSFC Grant No. 30930108 (W-S. F.); CAMS Innovation Fund for Medical Sciences 2016-I2M-1-010 (W-S. F.)

Author contributions: Conceptualization: A.E.P., W-S.F., M.O.S. and J.F.D. ; Investigation: A.E.P., K.B., T.M., N.O., D.L-A., M.A.O., F.J-P., K.G., J.F.G.A. C.R.,

644 J.F.D., A.C. J. E-G., S.K., Y.M. and S.L.; Visualization: A.E.P. and M.A.O. Writing—
645 original draft: J.F.D. Writing—review & editing: A.E.P., W-S.F., M.O.S., J.M.A. and K-
646 H.A.

647 **Competing interests:** Authors declare that they have no competing interests.

648 **Data and materials availability:** All raw data non presented in the manuscript are
649 available upon reasobable request from the authors. Cell biology, biochemistry, fiber
650 diffraction and NMR data requests should be addressed to J.F.D. Crystallographic data
651 requests should be addressed to A.E.P.

Figures and Tables

Table 1. IC50[1] values (μM) of tested compounds in Ptx sensitive KB (HeLa), HeLa S3 and in Ptx resistant KBV (HeLa) P-gp overexpressing and HeLa βIII-tubulin overexpressing cells.

Compound	KB μM	KBV μM	HeLa S3 μM	HeLa βIII μM
2a	0.6±0.1	>20	11.5±0.8	11.8±0.3
2b	10±3	>20	17.7±0.6	16.6±0.3
2c	13±1	>20	12.9±0.8	>20
2d	>20	>20	>20	>20
Ptx[2]	0.0019 ± 0.0001	9± 4	0.0011 ± 0.0004	0.034 ± 0.009

[1]IC50 values of growth inhibition in a panel of HeLa (KB and Hela S3) cervical carcinoma cells expressing P-glycoprotein (KBV) or the βIII isotype of tubulin (Hela βIII), compared to the isogenic parental lines. Values are presented as the mean±SE of three independent measurements[2]. Data from reference(*47*).

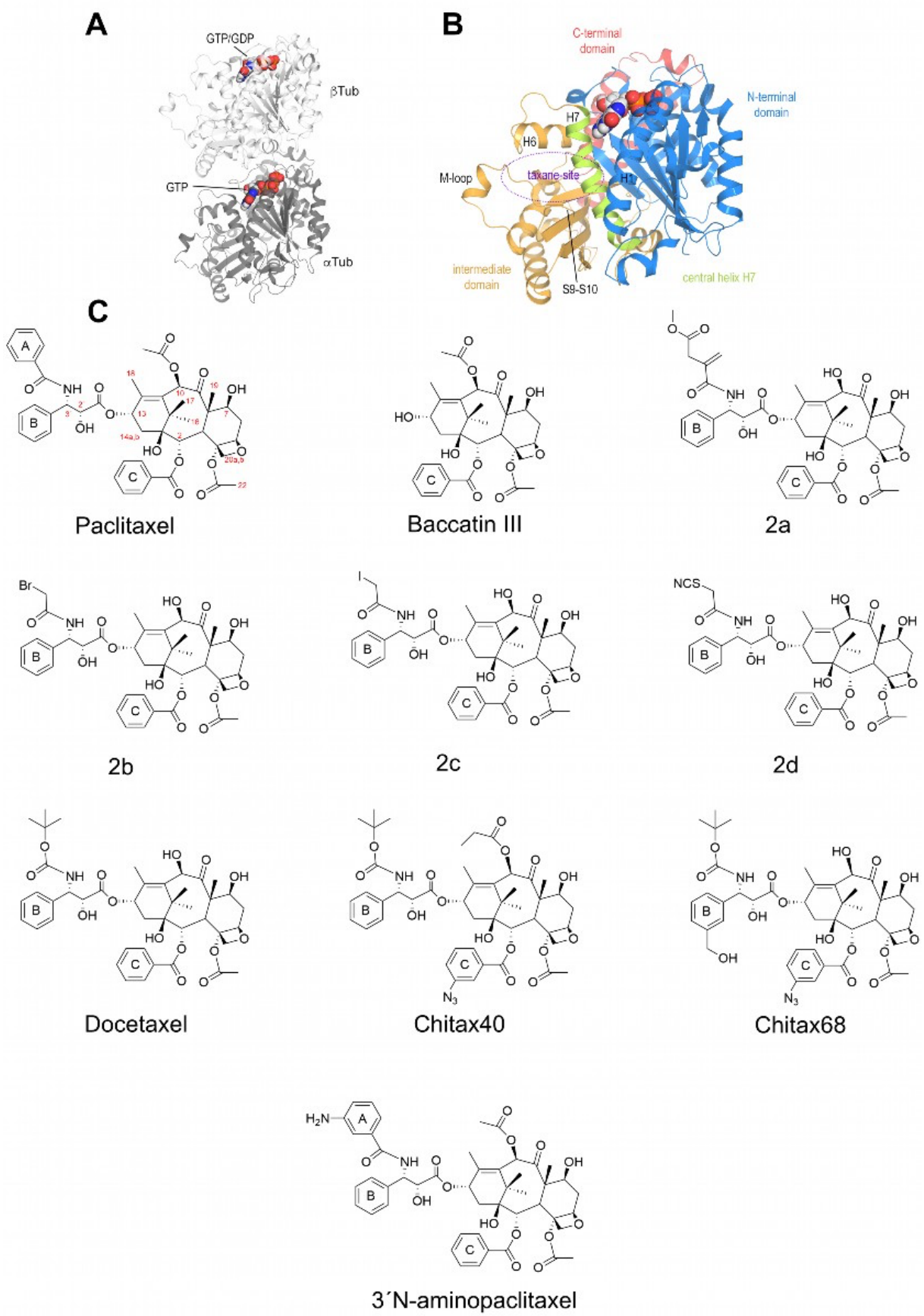

665

666 **Figure 1.** (**A, B**) Structural features of tubulin. (**C**) Structures of taxanes used in this

667 study.

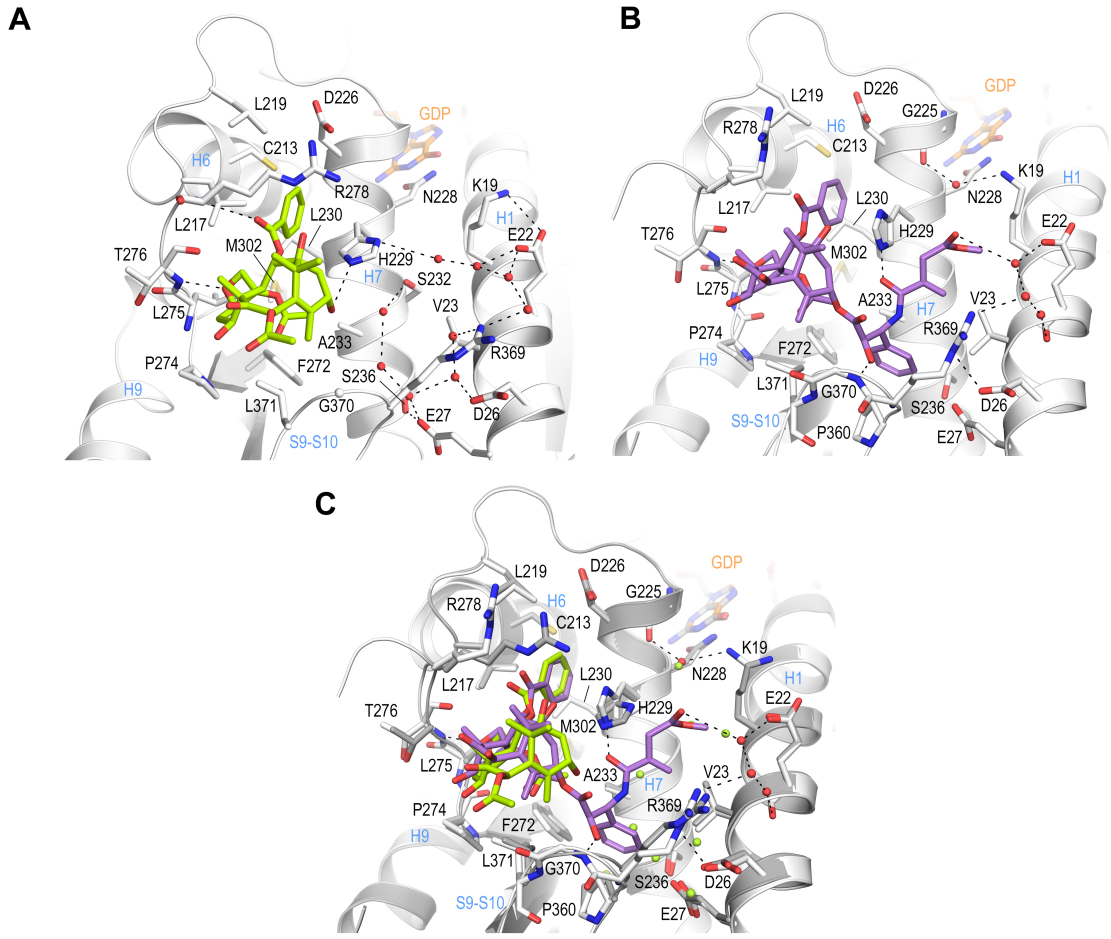

Figure 2. Crystal structure of T_2R-TTL-baccatin III (PDB ID 7A7I) and T_2R-TTL-2a (PDB ID 7A7F) complexes. (**A**) Close-up view of the interaction network observed between baccatin III (lemon) and tubulin (light gray). Interacting residues of tubulin are shown in stick representation and are labeled. Oxygen and nitrogen atoms are colored red and blue, respectively; carbon atoms are in lemon (baccatin III) or light gray (tubulin). Hydrogen bonds are depicted as black dashed lines. Secondary structural elements of tubulin are labeled in blue. (**B**) Close-up view of the interaction of **2a** (violet) with tubulin in the same view and representation as in (**A**). (**C**) The same close-up view as in (**A**) and (**B**) with the superimposed baccatin III (lemon) and **2a** (violet) complex structures. Water molecules belonging to the baccatin III structure are represented as lemon spheres.

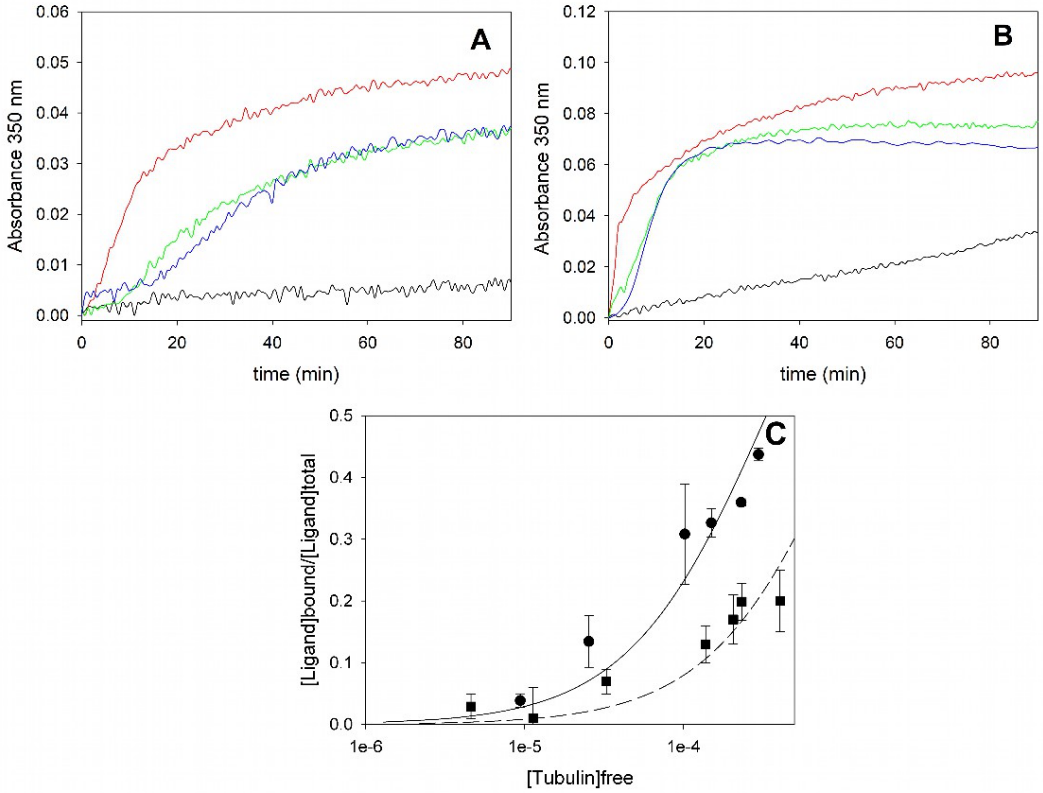

Figure 3. Biochemical characterization of the tubulin-2a and 2b interaction. Time-course assembly of 25 μM tubulin in 10 mM phosphate buffer, 1 mM EDTA, 1 mM GTP, pH 6.7, with 4 **(A)** or 7 mM **(B)** $MgCl_2$ in the presence of 27.5 μM Ptx (red), **2a** (green), **2b** (blue) or vehicle (DMSO, black). (**C**) Isotherm of binding of 50 μM baccatin III (circles and solid line) or **2a** (squares and dashed line) to tubulin. Error bars are standard errors of three independent measurements. Lines are the fitting to a single site model.

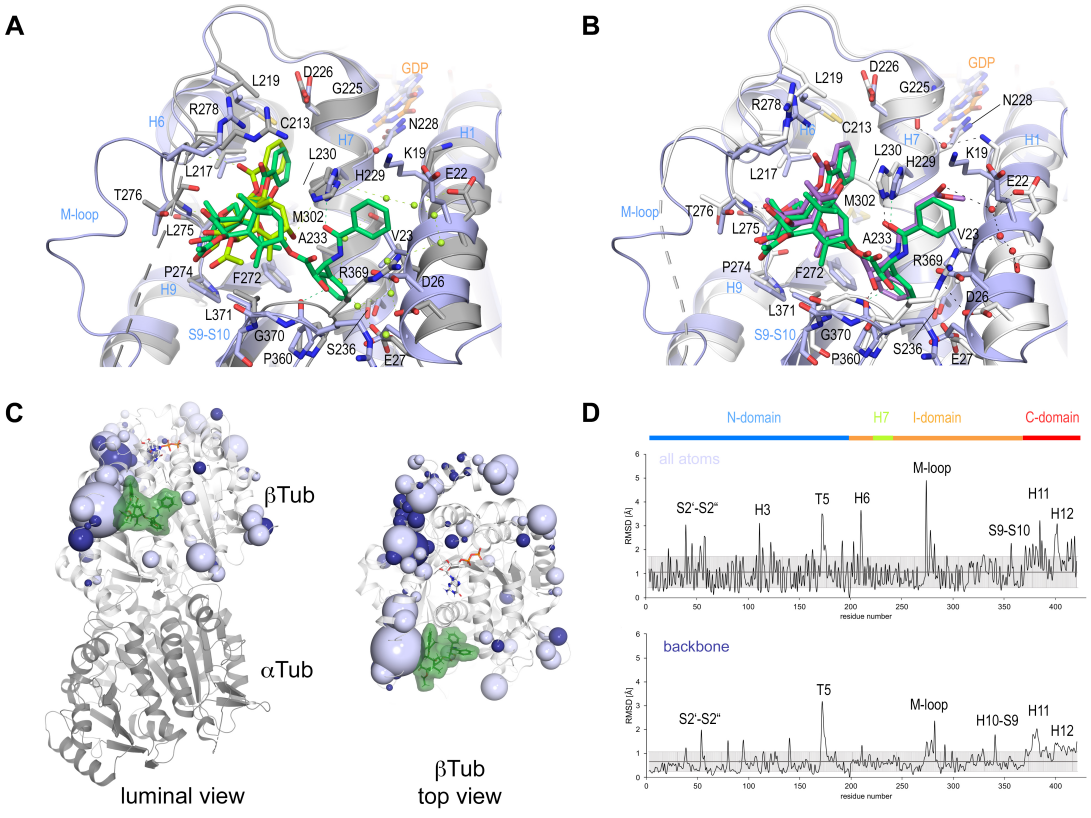

690

691 **Figure 4. Comparison of taxane binding to unassembled c- vs. assembled, s- tubulin.**
692 (**A**) Close-up view of the superimposed baccatin III bound (ligand in lemon; protein in
693 grey ribbon and sticks) to unassembled, c-tubulin and Ptx bound to assembled, s-tubulin
694 as found in a MT (PDB ID 6WVR; ligand in dark green; protein in slate ribbon and sticks)
695 structures. Interacting residues of tubulin are shown in stick representation and are
696 labeled. Oxygen and nitrogen atoms are colored red and blue, respectively. Hydrogen
697 bonds are depicted as black dashed lines. Secondary structural elements of tubulin are
698 labeled in blue. Water molecules belonging to the baccatin III structure are represented
699 as lemon spheres. The structures were superimposed onto their taxane-sites (residues
700 208–219 + 225–237 + 272–276 + 286–296 + 318–320 + 359–376; rmsd 0.894 Å (52 C_α
701 atoms). (**B**) Close-up view of superimposed **2a** bound to unassembled tubulin (ligand in
702 violet; protein in grey ribbon and sticks) and Ptx bound to assembled tubulin (PDB ID
703 6WVR; ligand in dark green; protein in slate ribbon and sticks) structures (rmsd 0.826 Å
704 (52 C_α atoms) using the same settings as in (**A**). (**C**) Perturbations on β-tubulin induced
705 by Ptx upon binding to assembled tubulin in MTs (PDB ID 6WVR). The α-tubulin and
706 β-tubulin chains are in ribbon representation and are colored in dark and light grey,
707 respectively. The rmsd differences between unbound and Ptx-bound, assembled MTs are
708 represented as light (all atom rmsd) and dark (backbone rmsd) blue spheres. Only the
709 rmsd-differences above a threshold of average ± standard deviation are displayed. The
710 sphere-radii correspond to the average-subtracted rmsd-values displayed in panel (**D**). (**D**)
711 rmsd plots of all atoms (top) and backbone (bottom) positions between the Ptx bound
712 (PDB ID 6WVR) and the apo (PDB ID 6DPV) assembled tubulin state in MTs. The grey
713 error bar represents the average rmsd ± standard deviation. The top bar is colored
714 according to the following domain assignment: N-domain (marine blue), I-domain
715 (orange), central helix βH7 (lemon) and C-domain (red). The β-tubulin chains of the
716 corresponding structures were superimposed onto their β-tubulin N-terminal β-sheets
717 (rmsd 0.304 Å 30 C_α).

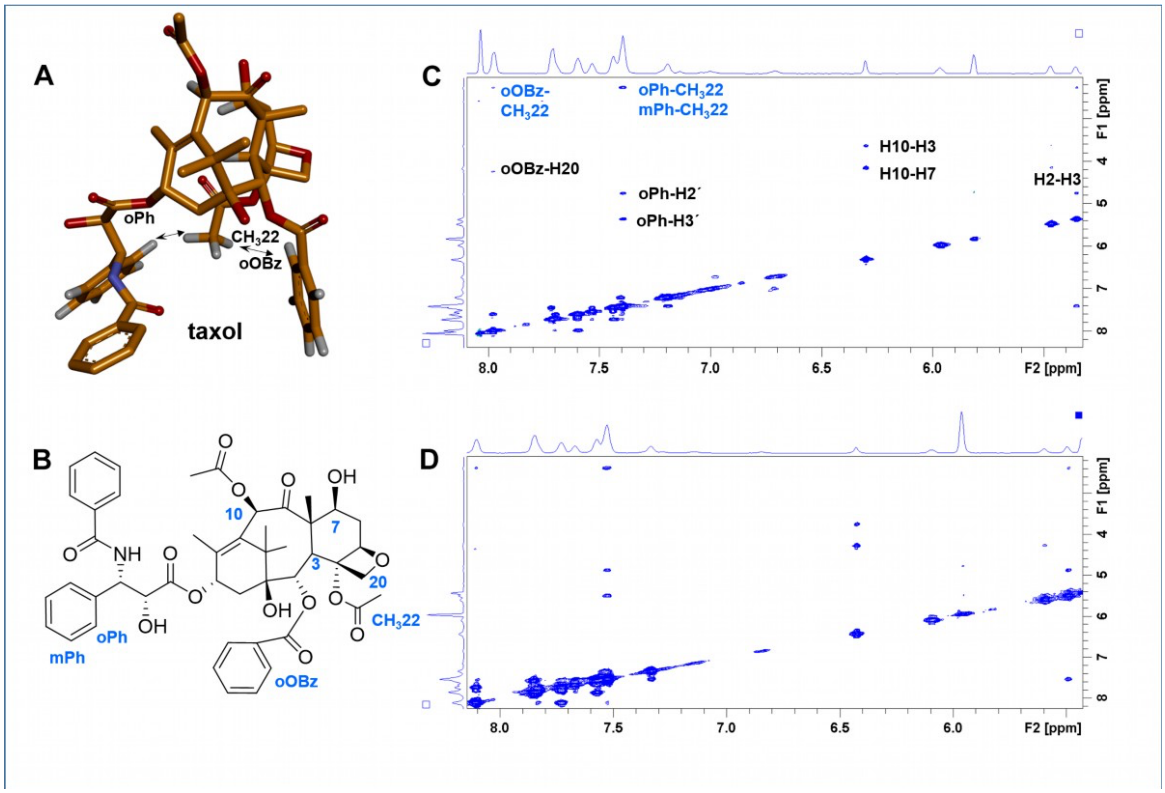

Figure 5. NMR-TR-NOESY characterization of the Ptx-tubulin interaction. (**A**) Bioactive structure of Ptx as determined by TR-NOESY. (**B**) Chemical structure of Ptx, indicating the protons involved in the TR-NOESY detected interactions. (**C**) TR-NOESY spectra (298 K) of Ptx bound to tubulin dimers. (**D**) TR-NOESY spectra (310 K) of Ptx bound to MTs.

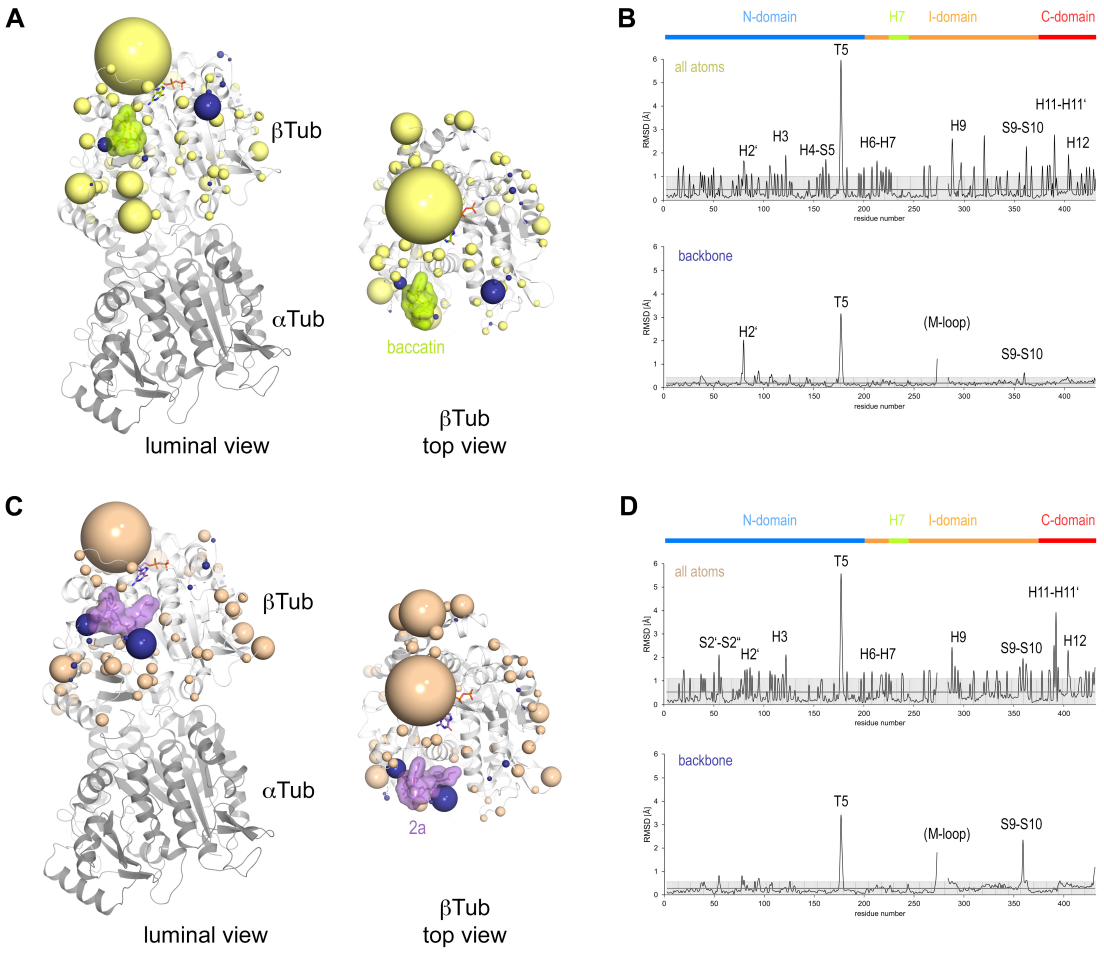

Figure 6. Perturbations induced by taxane binding to unassembled, c-tubulin. (**A**) Perturbations on all residue (yellow) and backbone atoms (dark blue) of the β-tubulin chain induced by baccatin III upon binding to unassembled tubulin. The tubulin chains are in ribbon representation and are colored in dark (α-tubulin) and light (β-tubulin) grey, respectively. The rmsd-values of the superimposed unbound and baccatin III bound, unassembled tubulin are represented as pale yellow (all atom rmsd) and dark blue (backbone rmsd) spheres, respectively. Only the rmsd-values above a threshold of average + standard deviation are displayed. The sphere-radii correspond to the average-subtracted rmsd-values displayed in panel (**B**). (**B**) rmsd plots of the all atoms (top) and backbone (bottom) positions between the baccatin bound and the apo (PDB ID 4I55) unassembled tubulin state. The grey error bar represents the average rmsd ± standard deviation. The top bar is colored according to the following domain assignment: N-domain (marine blue), I-domain (orange), central helix H7 (lemon), C-domain (red). The β-tubulin chains of the corresponding structures were superimposed onto their β-tubulin N-terminal β-sheet (rmsd 0.08 Å 29 C_α). (**C**) Perturbations on all residue (wheat) and backbone atoms (dark blue) of the β-tubulin chain induced by **2a** upon binding to unassembled tubulin. (**D**) rmsd plots of the all atoms (top) and backbone (bottom) positions between the **2a** bound and the apo (PDB ID 4I55) unassembled tubulin state (rmsd 0.10 Å of 29 C_α). The same display settings as in (**B**) are applied.

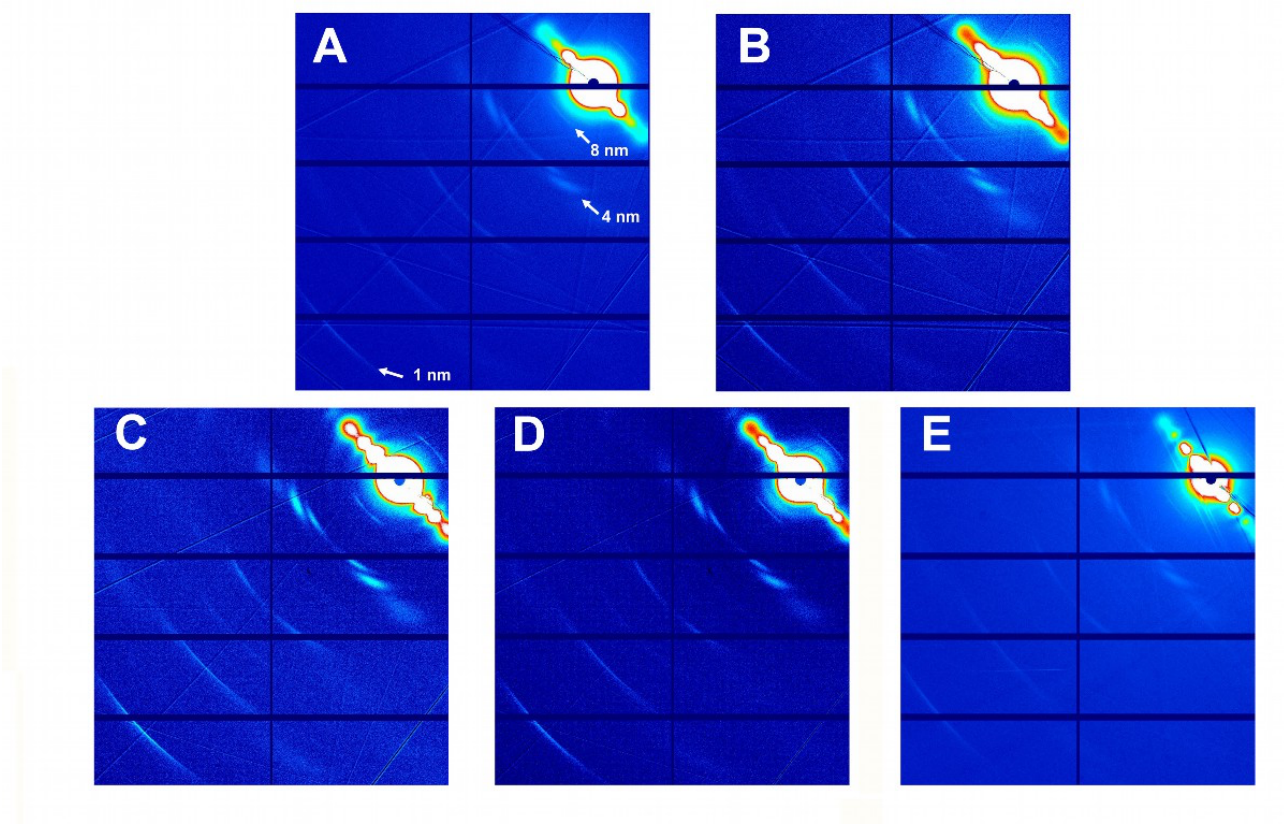

749 **Figure 7. Fiber diffraction patterns of MTs assembled from** (**A**) GTP-tubulin and Ptx,
750 (**B**) GTP-tubulin and Dtx, (**C**) GTP-tubulin and **2a**, (**D**) GTP-tubulin and **2b**, and (**E**)
751 GTP-tubulin and baccatin III.
752

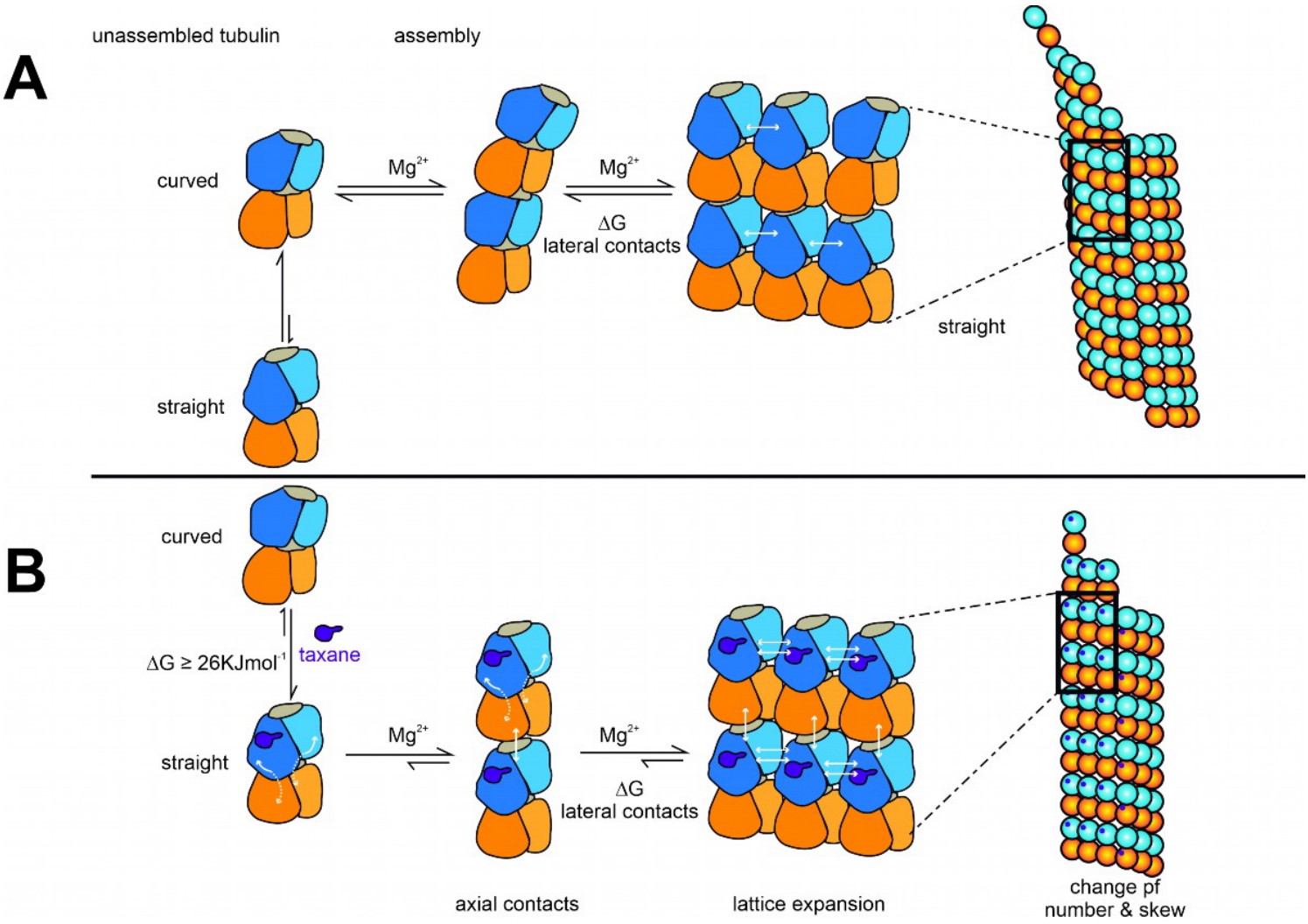

753

754 **Figure 8. Schematic representation of the mechanism of taxane-induced MT**
755 **assembly**. **(A)** MT assembly scheme with a classical bidimensional nucleus for
756 cooperative polymerization. **(B)** Taxane-induced MT assembly scheme with an activated,
757 s-tubulin for cooperative polymerization. In both panels, α-Tubulin is in orange (Nt-
758 domain light orange and, intermediate domain dark orange), β-tubulin is in blue
759 (Nt-domain light blue and, intermediate domain dark blue), while the nucleotide binding
760 site in tubulin is in gray. Taxane molecules in (B) are depicted in purple. White arrows
761 show direct and allosteric protein-protein interactions.

762

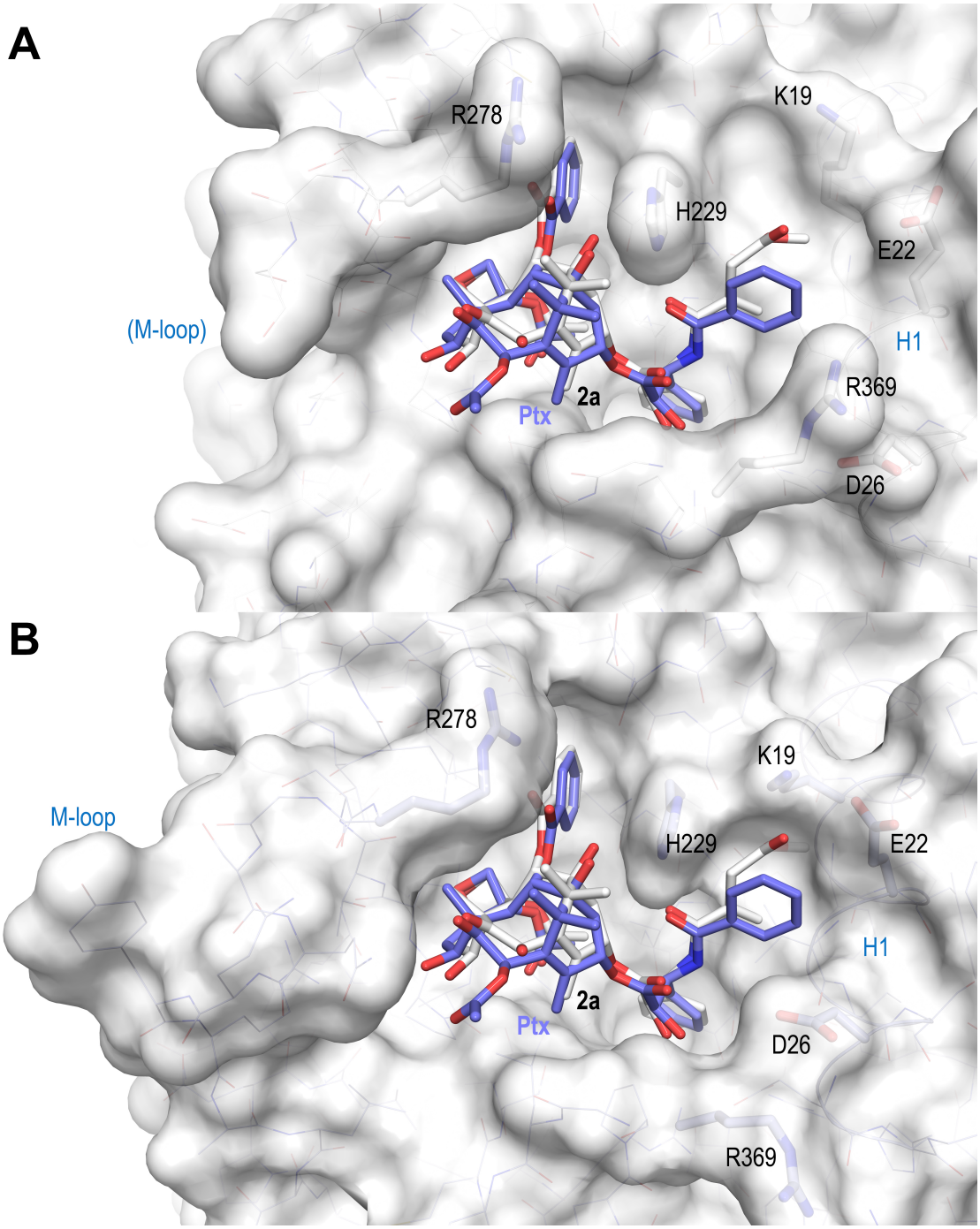

Figure 9. Surface representations of liganded taxane sites in both (A) the c- and (B) s-tubulin conformational state. The structures of **2a** (white) and Ptx (slate) bound to MTs (PDB ID 6WVR) were superimposed onto their central helices βH7. The side chains of the βM-loop residue βR278 and of residues surrounding the C13 side chains of the ligands are in stick representation and are labeled. Helix βH1 is highlighted in ribbon representation